WEAK BOND DETECTION IN SINGLE-LAP SHEAR BONDS BY EVALUATING VIBROACOUSTIC MODULATIONS WITH ARTIFICIAL NEURAL NETWORKS

Benjamin Boll[a], Erik Willmann[a], Bodo Fiedler[a], Robert Horst Meissner[a,b]

a: Institute of Polymers and Composites, Hamburg University of Technology, Hamburg
b: Institute of Surface Science, Helmholtz-Zentrum Hereon, Geesthacht, Germany
*benjamin.boll@tuhh.de

Abstract: *Adhesive bonding is an essential method for joining composite materials. However, the occurrence of contaminations, resulting in a not detectable weakened adhesion, persists. This study aims to uncover weak bonds with the vibroacoustic modulation method, a nonlinear ultrasonic testing method, where ultrasonic guided waves are modulated by a simultaneously applied, high amplitude pump wave. Afterwards, the measurements are evaluated by a deep learning approach. A previous dataset of 40 single-lap shear specimens (ASTM D5868-01), in which artificial interfaces in the form of circular PTFE films or release agent contaminations were introduced, was extended by a second dataset with 14 specimens of a different laminate to evaluate the robustness and transferability of the method. The proposed neural network approach can reliably recognize the bonding flaws in the training dataset and even has high accuracies on the transfer dataset, demonstrating the tremendous potential for the nondestructive evaluation of adhesive joints.*

Keywords: Composites; Weak bonds; Nondestructive Testing; Vibroacoustic Modulation; Artificial Neural Networks

1. Introduction

The application of fiber-reinforced composites for primary structures is widely adopted due to their high specific strength, corrosion resistance, and fatigue properties. Nevertheless, the lightweight potential for bonding composite structures is not fully exploited since the traditional bonding with bolts or rivets introduces substantial stress concentrations around the fastener and, therefore, requires a thickened material [1]. Adhesive bonding overcomes these difficulties due to the homogeneous stress concentration in the bonding area [1,2]. However, even with highly automated processes, contaminations persist, resulting in areas of weekend adhesion. Since the weakened bond arises from a changed chemical interaction, magnitudes smaller than ultrasonic wavelengths [3], they are hard or even impossible to detect with conventional nondestructive testing. The significant reduction of bond strength, coupled with the inability to detect these defects, poses a severe threat to structural safety and limits the lightweight and application potential [2,4].

Numerous studies have been published where weak bonds are created artificially either by contaminating the adherent's surface [5–7] or by introducing a non-adhesive film [5,8–10]. While the non-adhesive film is detectable by several NDT methods [5,6,8], the release agent contamination resembles reality much closer [11] and is more challenging to detect. To the author's knowledge, there is no method capable of reliably detecting areas of reduced adhesion, preventing the application of adhesives as the main bonding method in primary structures [1,4,12,13]. In this regard, applying nonlinear ultrasonic methods has shown promising results

  doi:10.5075/epfl-298799_978-2-9701614-0-0

in the literature. The vibroacoustic modulation (VAM)—which combines nonlinear ultrasonic measurements with a simultaneously introduced vibration— has shown a superior sensitivity to damages already on other specimen types [6,14–16].

Our prior work [17] showed the ability to detect weak bonds in single lap shear specimens. An artificial neural network evaluated the VAM measurements to classify the bonding state. This combination has proven superior to the traditional VAM evaluation based on a damage index. In recent VAM-related works, the nonlinear modulation—indicating the damage—is divided into amplitude and phase modulation. In this work, we quantify whether—based on our extended dataset—a weak bond detection, evaluating only these modulation values results in precise predictions as well. Furthermore, the transferability and robustness of the old and newly trained ANNs are evaluated on the newly manufactured specimen with a different laminate layup.

2. Introduction

2.1 Specimen manufacturing

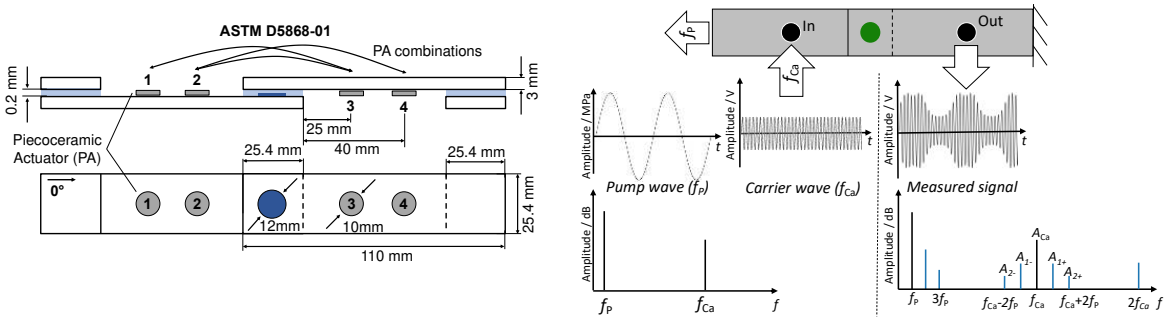

Figure 1. Dimensions of the tested specimen (left). The gray disks illustrate the different positions of the piezoceramic actuators. Illustration of VAM (right), where the excitation signals on the left result in the modulated signal with higher harmonics and sidebands (adapted [17]*).*

Additionally to the 40 original specimens (details in [17]), 14 specimens were manufactured according to the same procedure but with a different laminate layup. In contrast to the 3mm $[0_4]$s glass fiber laminate, the new specimens were made from a 3 mm thick adherent with a $[0,\pm45_3]_s$ layup. The same E-glass fibers and the low-viscosity epoxy system (RIMH135 with RIMR137 from Hexion) have been used. The single-lap joints are produced in a secondary-bonding process with the 2C-epoxy adhesive (Sika-Power-1280). The dimensions follow the ASTM D5868-01, as shown in Figure 1 (left). Prior to the bonding process, seven specimens were contaminated with a release agent (RA) (Mikon W-64+ from Münch Chemie) in a circular area (d=12 mm), creating nondetectable weak bonds in ultrasonic C-Scans. Since the PTFE intrusions are detectable with VAM [6,17] and traditional testing methods (e.g. ultrasonic testing), only the RA and pristine specimens were newly manufactured and compared.

2.2 Vibroacoustic modulation method

The vibroacoustic modulation (VAM) is an active nonlinear ultrasonic method for nondestructive testing. It utilizes the modulation of two sinusoidal frequencies. The *pump wave* has a low-frequency f_P but high amplitude to alter the stress state in the specimen, especially around defects. The *probe wave* with the high-frequency f_Ca acts as a carrier for the modulated signal

  doi:10.5075/epfl-298799_978-2-9701614-0-0 published under CC BY-NC 4.0 license

[14]. Damages (initial defects, i.e., discontinuities, surfaces, interfaces, etc.) and presumably the weak bonds of this work result in a nonlinear modulation of the carrier [15–17].

Traditionally, VAM is evaluated by calculating the frequency domain from the steady-state signal with the Fast Fourier transform (FFT). The nonlinear behavior of the specimen results in a superposition of several dominating frequencies. They can be attributed to the unmodulated frequencies at f_{P} and f_{Ca}, the higher harmonics due to the modulation $(nf_{\mathrm{P}} \wedge nf_{\mathrm{Ca}} \mid n \in \mathbb{N})$, and sidebands around the carrier frequency $(f_{\mathrm{Ca}} \pm nf_{\mathrm{P}} \mid n \in \mathbb{N})$ [14] as shown in Figure 1 (right). For evaluation, a representative value such as the Modulation Index (MI) is calculated from the amplitudes of the carrier signal and first sidebands denoted as A [18,19].

$$MI = 20 \cdot log_{10}\left(\frac{A_{1+}+A_{1-}}{2 \cdot A_{\mathrm{Ca}}}\right) \quad (1)$$

In recent works, the separation in amplitude modulation (AM) and phase modulation (PM) was shown to be beneficial and attributed to different types of damage, which in turn increased the sensitivity of VAM. This separation was proposed by methods like the Hilbert-transform [20], the Hilbert-Huang-transform [21], the In-phase/Quadrature Homodyne Separation (IQHS) [22], and the short-time Fourier-transform (STFT) [23]. Since the STFT provides a significant advantage of the lowest computational cost, which is beneficial for the real-world application in sensor networks, in the following we analyze whether it could be used for weak bond detection.

Most works analyze the development of the MI over the specimen lifetime, where the first measurement is defined as a baseline. However, comparing measurements from different specimens leads to severe differences in signal strength and initial modulation, making evaluations a complex endeavor. Hence, as presented later, the data-driven analysis proves beneficial for such complex and highly correlated input data.

2.3 Experimental setup

To have similar conditions for all measurements, all vibroacoustic measurements were performed on a servo-hydraulic testing machine (Instron 8801 with a max. load capacity of 63 kN). The pumping frequency was chosen as 5 Hz with an amplitude of 11 MPa and a stress ratio of $R = 0.1$ due to limitations on the hydraulic valve of the machine and the tensile strength of the specimen. The high-frequency ultrasonic vibration was introduced by piezoceramic actuator disks (PI-Ceramics 10 x 2mm) attached to the specimen with double-sided tape (Tesa 56172). A NI-USB 6366 (National Instruments) with a sampling rate of 2 MS/s was used for the excitation and monitoring of the piezoceramics. The generated sine was amplified to 12 $V_{pp,}$ and 39 equidistant measurements in a range of 200 kHz <f_{Ca}< 220 kHz and a duration of 2 s were acquired. Furthermore, as shown in Figure 1, the signal path between actuating and receiving piezoceramic was alternated, resulting in a total of 234 VAM samples per specimen (39 frequencies, three pathways, two directions).

2.4 Machine Learning Application

As preprocessing, the transient regime (first 0.4 ms) of all measurements was removed. The remaining signal (1.996 s) was multiplied with a Hanning window function and afterwards transformed with a fast Fourier transformation (FFT) into the frequency domain. This procedure resulted in a reduction of spectral leakage and clearly pronounced sideband peaks in the frequency domain. For each specimen j, the amplitude of the sidebands $A_{j,i\pm}$ and the carrier

  doi:10.5075/epfl-298799_978-2-9701614-0-0

amplitude $A_{j,\mathrm{Ca}}$ are stored in a data matrix denoted as $\mathbf{X_{SB}}$ for the initial and $\mathbf{X_{Transf}}$ for the newly manufactured specimen. The bonding type is stored as the label for the classification in vectors denoted as $\boldsymbol{y}$ and $\boldsymbol{y}_{\mathbf{Transf}}$. All amplitudes in dB-scale were normalized so that the mean value was set to zero and the standard deviation equals one (Z-score normalization). This normalization was calculated for the training set and adapted for the validation set and $\mathbf{X_{SB}}$. For a second dataset $\mathbf{X_{APM}}$, the amplitude modulation $\mathrm{m_{j,A}}$ and phase modulation $\mathrm{m_{j,P}}$ were calculated based on the STFT [23].

The defect detection is implemented as a classification problem in TensorFlow. The optimal network architecture for the dataset $\mathbf{X_{SB}}$ was determined in a randomized grid search as described in [17]. Here, the number of used sidebands as ANN-input, the frequency range, and the signal path of the measurements were permuted to identify whether some frequencies or placements of the piezoceramics resulted in more precise predictions. These results are compared to a smaller network (ANN 2) with 16 neurons in one hidden layer (2-16-3 neurons) trained on $\mathbf{X_{APM}}$.

All models were evaluated by calculating the accuracy of each prediction, which is defined as $\mathrm{accuracy}(\boldsymbol{y}, \hat{\boldsymbol{y}}) = \frac{1}{n}\sum_{i=1}^{n} 1_{\boldsymbol{y}_i}(\hat{\boldsymbol{y}}_i)$ where n is the number of samples, $\hat{\boldsymbol{y}}_i$ is the predicted label of the i-th sample, $\boldsymbol{y}_i$ is corresponding true label, and $1_{\boldsymbol{y}_i}(\hat{\boldsymbol{y}}_i)$ is the indicator function which returns one if both match and zero otherwise.

Since the dataset is rather small for the training of deep ANNs, the dataset splitting in the training set (80%) and validation set (20%) influences the result. Therefore, every shown result from an ANN is the mean of 10 randomized splits. In every split, all measurements of a specimen are either in the test or validation set, as this has been shown to increase the reliability of the results [17].

3. Results and Discussion

3.1 Vibroacoustic measurements

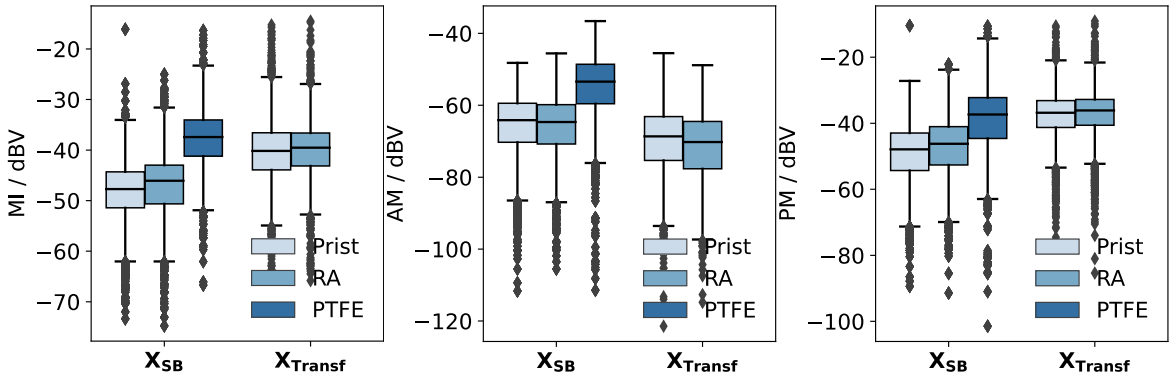

Figure 2. Boxplots for the Modulation index (left), amplitude modulation (middle) and phase modulation (right).

The vibroacoustic measurements are typically evaluated by calculating the "traditional" MI, as shown in Figure 2 (left). Here, the MI is plotted for the 239 measurements of all specimens in a boxplot. Indicated by the median value (line inside each box), a differentiation of the PTFE specimen of $\mathbf{X_{SB}}$ is possible even though the standard deviation and interquartile range are relatively high. However, the release agent specimen cannot be differentiated from the pristine

  doi:10.5075/epfl-298799_978-2-9701614-0-0 published under CC BY-NC 4.0 license

specimens based on the MI. The mean MI of the new dataset $\mathbf{X_{Transf}}$ is significantly higher compared to $\mathbf{X_{SB}}$ and closer to the mean of the PTFE specimens, underlining the importance of more values to be analyzed.

Therefore, also the values of the amplitude and phase modulation calculated with the STFT are presented. For both values, the modulation of the PTFE specimen is the highest. However, the mean AM of the RA specimens is slightly lower and the mean PM is marginally higher compared to pristine specimens. However, both differences are negligibly compared to standard deviation.

3.2 Adhesive Bonding Classification

To outperform the bond differentiation based on a pure MI evaluation or other indices, shown in the previous chapter, more sophisticated data-driven methods were applied to predict the bonding. As described in the methods section, we have created two datasets from the measurements, where $\mathbf{X_{SB}}$ contains the normalized sideband values and $\mathbf{X_{APM}}$ contains the calculated AM and PM value of the signal obtained with the STFT transform. Since the measured frequency range is rather big, the ANNs were trained on subsets of 5 neighboring frequencies of one piezo combination. The most precise results of the 10-fold cross-validation are shown in Figure 3. Note that the used carrier frequency ranges overlap. Hence, each point represents the highest achieved accuracy of a frequency obtained for training an ANN with input data from a certain frequency range.

The ANNs trained on the actual sideband values ($\mathbf{X_{SB}}$) were able to predict the bonding type reliably. The differentiation between the three classes of specimens is possible with an accuracy of 93.4 % if the frequency range of 202.5 − 204.5 kHz and the number of five sidebands on both sides and the carrier are used (as marked with the red circles). As discussed in [17], the accuracy of the prediction depends on the number of sidebands used as input for the ANN. Less evaluated sidebands result in lower accuracies due to less information as ANN input. However, a high number of used sidebands results in the ANN overfitting the existing noise. Hence, this number has to be chosen carefully. Furthermore, the accuracy is also dependent on the placement of the piezoceramic. The asymmetric combinations (P1–P3 and P2–P4) result in high accuracy and strong frequency dependence compared to the symmetric layout (P2–P3). This might be an effect of the distance to the bond, the signal path length, or more generally the resulting eigenmodes of the specimen.

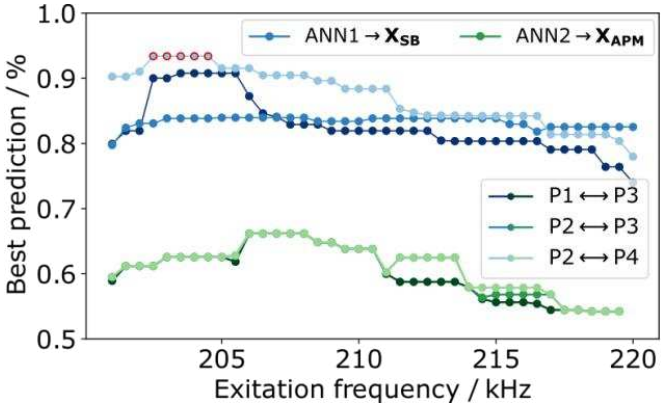

Figure 3. Comparison of the maximal achieved bond line defect classification for different signal pathways between the piezoceramics and probe frequencies. Compared are the results for the ANNs trained on $\mathbf{X_{SB}}$ and $\mathbf{X_{APM}}$.

  doi:10.5075/epfl-298799_978-2-9701614-0-0 published under CC BY-NC 4.0 license

When training the ANNs solely on the AM and PM values ($\boldsymbol{X_{APM}}$) extracted by the STFT, the accuracy of the prediction is less accurate compared to the networks trained on the peak values. Only a maximal accuracy of 67 % was reached with a maximal value around 206-208 kHz. Comparable to the prior results, a dependency on the utilized frequency range is observable as well. Nevertheless, the precision of the different piezo combinations is mostly similar. This significantly worse behavior can have a variety of reasons. Most importantly, the STFT is based on the assumption of a perfect sinusoidal modulation, which might be close but not exactly the predominant stress-strain response of the specimens. Furthermore, the STFT evaluates only frequency components of f_{P} and f_{Ca}. However, as many publications describe, higher harmonics also occur as a nonlinear response to damages. Since VAM is evaluated at the steady state of the vibration, these higher harmonics are also reflected many times in the specimen and, in turn, contribute to the higher-order sidebands as well. For example, the first harmonic at 10 Hz would contribute to the second, fourth, and sixth sidebands, the second harmonic in the third and sixth. These contributions are not taken into account by the STFT. Finally, the networks applied on $\mathbf{X_{APM}}$ are smaller compared to $\mathbf{X_{SB}}$ since patterns in two input values are much easier to detect and bigger networks overfit the data resulting in even worse results.

Interestingly, interchanging the left and right sidebands of the $\mathbf{X_{SB}}$ evaluation dataset results in a mean accuracy decrease of around 28 %. This underlines the relevance of the asymmetries in the sideband peaks and results in a similar accuracy comparable to the AM and PM ANN training ($\mathbf{X_{APM}}$), which—as an approximation—does not take all frequency components into account.

3.3 Transfer of trained models to the new dataset

Based on the most accurate prediction of $\mathbf{X_{SB}}$ (piezo combination P2–P4, the frequency range of 202.5 − 204.5 kHz, amplitudes of 5 sidebands to each side and of the carrier as input, marked as red circles in Figure 3), 50 new ANNs have been trained and saved with randomized splits into test and training data of $\mathbf{X_{SB}}$ to evaluate whether the "learned" patterns are universal and also applicable to the specimen with a changed laminate layup in $\mathbf{X_{Transf}}$. The number of trained networks is increased compared to the prior results to further test the robustness. These networks reach a mean accuracy of 92,5 %, which is 0.9 % below the results from the previous chapter due to statistical reasons of the small dataset, but still underlining the good agreement.

These networks were now used to predict the bonding state of $\mathbf{X_{Transf}}$. The combined predictions are shown in Figure 4 in a confusion matrix. Note that no PTFE specimens have been tested, resulting in only two rows. However, the networks were trained as ternary classification and misclassified a marginal percentage of samples as PTFE specimens, as shown in the left column.

The upper-middle and lower-right boxes represent the percentage of correct predictions, while the other indicates the wrong predictions. In total, an accuracy of 72.9 % was achieved. However, the confusion matrix indicates that the networks tend to classify specimens as contaminated, resulting in higher accuracy for the release agent specimen than the pristine ones. This could stem from the lower stiffness and therefore changed wave propagation of the new composite layup. Furthermore, the high count of fibers in a $\pm$45° direction influences the Lamb waves. As discussed by [24], a continuous mode conversation (S to A mode) occurs in composites made with twill fabric and possibly other layups. These factors eventually change

  doi:10.5075/epfl-298799_978-2-9701614-0-0

the measured signal, resulting in slight changes in the modulation, which probably explain the near 20% reduction in accuracy.

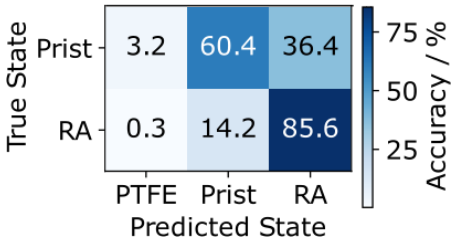

Figure 4. Confusion matrix of the 50-fold prediction of X_{Transf} with ANNs trained on $\mathbf{X_{SB}}$.

4. Conclusion

The evaluation of the vibroacoustic measurements with a machine learning approach, as presented in this work, has shown promising capabilities for detecting a reduced adhesion by release agent contaminations (or more general weak bonds). The results indicate that the nonlinear modulation of ultrasonic waves can detect defects or adhesive properties in the interface between adhesive and substrate [19], although the wavelength is in the cm range and, therefore, considerably larger than the adhesive layer thickness. The enhanced sensitivity is most likely related to the interaction of the cyclic stress change in the bond by the high-stress pump frequency and the Lamb-wave characteristics. Larger contaminated regions are likely to boost the signal's nonlinear amplitudes, improving ANN accuracy, although contaminations smaller than the Lamb wavelength may be more difficult to detect.

However, just training a network on the extracted values of amplitude and phase modulation results in a severe decrease in the reached accuracy. This decrease indicates that the information in the sideband amplitudes and the carrier are not completely included in the STFT calculations. For example, interchanging the inputs of the most accurate ANN trained on $\mathbf{X_{SB}}$ by swapping left and right sidebands results as well in an average decrease in classification accuracy of 28 %, which is in the range of the predictions on $\mathbf{X_{Transf}}$.

Predicting the contamination of specimens with the same dimensions but different layup shows a decrease in accuracy as well. Presumably, the changes in the laminate structure result in altered wave propagations and further effects like a continuous mode conversation of the lamb waves. Despite these effects, the ANNs trained on $\mathbf{X_{SB}}$ were still able to predict the bonding state of $\mathbf{X_{Transf}}$ reasonably well with a more reliable detection of contaminated specimens (86 %) while misclassifying roughly 40 % of the pristine specimens.

To conclude, this supervised ANN approach is suitable for analyzing similar specimens, e.g., in mass productions. Hence, the change in specimen dimensions, design, or manufacturing reduces prediction quality. However, the examined specimen with the different laminate could be classified with an accuracy far beyond a random guess.

5. References

1. Breuer. Commercial aircraft composite technology. Commercial Aircraft Composite Technology. 2016. 1–257 p.
2. Ehrhart, Valeske, Muller, Bockenheimer. Methods for the Quality Assessment of Adhesive Bonded CFRP Structures - A Resumé. AIP Conf Proc. 2010;44(3):1–8.

  doi:10.5075/epfl-298799_978-2-9701614-0-0

3. Brotherhood, Drinkwater, Dixon. The detectability of kissing bonds in adhesive joints using ultrasonic techniques. Ultrasonics. 2003;41(7):521–9.
4. Schmid Fuertes, Kruse, Körwien, Geistbeck. Bonding of CFRP primary aerospace structures - Discussion of the certification boundary conditions and related technology fields addressing the needs for development. Compos Interfaces. 2015;22(8):795–808.
5. Wood, Charlton, Yan. Ultrasonic evaluation of artificial kissing bonds in CFRP composites. e-Journal Nondestruct Test. 2014;19(12):1–10.
6. Chen, Soh, Lee, Tay, Tan. A vibro-acoustic modulation method for the detection of delamination and kissing bond in composites. J Compos Mater. 2016;50(22):3089–104.
7. Nagy. Ultrasonic classification of imperfect interfaces. J Nondestruct Eval. 1992;11(3–4):127–39.
8. Jairaja, Naik. Weak bond effects in adhesively bonded joints between the dissimilar adherends. J Adhes. 2019;00(00):1–23.
9. Ren, Lissenden. Ultrasonic guided wave inspection of adhesive bonds between composite laminates. Int J Adhes Adhes. 2013;45:59–68.
10. Heidarpour, Farahani, Ghabezi. Experimental investigation of the effects of adhesive defects on the single lap joint strength. Int J Adhes Adhes. 2018;80:128–32.
11. Harder, Florian. Localised Weak Bonds in Scarf Bonded CFRP Repairs - A Study of the Size and Location Dependence under Consideration of Hot-Wet Conditioning. 2019;
12. Heilmann. Qualitätskontrolle von Reparaturklebungen an Faserverbundstrukturen durch vollflächige Festigkeitsprüfung. 2020;
13. U.S. Department of Transportation. Federal Aviation Administration, Federal Aviation Administration. Advisory Circular Advisory Circular. Aviation. 2012;1(AC 25.1529-1A):1–2.
14. Pieczonka, Klepka, Martowicz, Staszewski. Nonlinear vibroacoustic wave modulations for structural damage detection: an overview. Opt Eng. 2015;55(1):011005.
15. Lim, Sohn. Necessary conditions for nonlinear ultrasonic modulation generation given a localized fatigue crack in a plate-like structure. Materials (Basel). 2017;10(3).
16. Pieczonka, Klepka, Dziedziech, Broda, Packo, Martowicz, et al. Nonlinear acoustics for structural health monitoring - Classical vs. non-classical approaches. 8th Eur Work Struct Heal Monit EWSHM 2016. 2016;1(July):1–12.
17. Boll, Willmann, Fiedler, Meißner. Weak adhesion detection – Enhancing the analysis of vibroacoustic modulation by machine learning. Compos Struct. 2021;273.
18. Zagrai, Donskoy, Chudnovsky, Golovin. Micro-and macroscale damage detection using the nonlinear acoustic vibro-modulation technique. Res Nondestruct Eval. 2008;19(2):104–28.
19. Dorendorf, Lalkovski, Rutner. Physical explanation for vibro-acoustic modulation due to local and global nonlinearities in a structure and its experimental and numerical validation. J Sound Vib. 2022;116885.
20. Ooijevaar, Rogge, Loendersloot, Warnet, Akkerman, Tinga. Vibro-acoustic modulation–based damage identification in a composite skin–stiffener structure. Struct Heal Monit. 2016;15(4):458–72.
21. Hu, Staszewski, Hu, Jenal, Qin. Crack detection using nonlinear acoustics and piezoceramic transducers-instantaneous amplitude and frequency analysis. Smart Mater Struct. 2010;19(6).
22. Donskoy, Ramezani. Separation of amplitude and frequency modulations in Vibro-Acoustic Modulation Nondestructive Testing Method. 2018;045002:045002.
23. Oppermann, Dorendorf, Rutner, Renner. Nonlinear modulation with low-power sensor networks using undersampling. Struct Heal Monit. 2021;(January).
24. Mook, Willberg, Gabbert, Pohl. Konversion von Lambwellen in CFK-Platten. DACH-Tagung der Dtsch Österreichischen und Schweizerischen Gesellschaft für Zerstürungsfreie Prüfung, 17-1992012 Graz. 2012;BB 136-CD:1–9.

  doi:10.5075/epfl-298799_978-2-9701614-0-0